

ARTICLE OPEN



Piezoelectric strain sensor with high sensitivity and high stretchability based on kirigami design cutting

Young-Gyun Kim^{1,2,5}, Ji-Hyeon Song^{3,5}, Seongheon Hong¹ and Sung-Hoon Ahn^{1,4}✉

Wearable technology requires high-performance sensors with properties such as small size, flexibility, and wireless communication. Stretchability, sensitivity, and tunability are crucial sensor properties; stretchability and sensitivity ensure user comfort and accurate sensing performance, while tunability is essential for implementing sensors in diverse applications with different ranges of motion. In this study, we developed a high performance kirigami piezoelectric strain sensor. Using finite element analysis, the sensing performance was evaluated, and the kirigami patterns were optimized. The electromechanical properties of sensors with four different kirigami patterns were analyzed. A sensor voltage measurement circuit was also designed, amplifying the output voltage 86.5 times by improving measurement accuracy. A piezoelectric kirigami sensor was constructed with a sensitivity of 9.86 V/cm² and a stretchability of 320.8%, higher than those of previously reported kirigami piezoelectric strain sensors. Finally, the fabricated sensor was successfully applied in a haptic glove for playing musical instruments.

npj Flexible Electronics (2022)6:52; <https://doi.org/10.1038/s41528-022-00186-4>

INTRODUCTION

Wearable sensors are becoming increasingly important in various applications such as health monitoring and artificial reality (AR)/virtual reality (VR) technology. Flexibility and stretchability are required for human body applications, and the demand for such sensors is increasing¹. Additionally, it is crucial to optimize sensor performance according to the target application because different sensor properties, such as stretchability and sensitivity, are required depending on the body part and application. For example, a sensor attached to an elbow requires higher stretchability than that required for a finger. Pulse sensing requires higher sensitivity than detection of bending motion. Therefore, it is essential to develop sensors with tunable sensing performance.

The sensing mechanisms for stretchable sensors are piezoresistive^{2–6}, piezocapacitive^{7–9}, and piezoelectric^{10–14}, with the piezoelectric mechanism being the most advantageous. Piezoelectric-based sensors can accurately measure rapid strain changes without latency. Unlike piezoresistive sensors, active sensing is possible with piezoelectric sensors. The output voltage produced with strain can be used as a power source for additional functions such as wireless communication. Therefore, piezoelectric materials are promising for strain sensing applications.

However, piezoelectric materials for strain sensing applications have two drawbacks that limit their applications, primarily to pressure sensors. First, the generated voltage dissipates to the surroundings such that the voltage peak appears only for a short duration when the strain is applied. This prevents utilization of piezoelectric materials in strain sensing applications because it is difficult to measure a transient output voltage. The voltage drop is mainly due to the measurement circuit. In addition, the measurement system cannot follow the rapid increase in voltage; thus, it cannot fully measure the actual voltage generated by the piezoelectric materials. Therefore, it is necessary to improve the

measurement circuit design of piezoelectric strain sensors. Second, piezoelectric materials with high piezoelectric coefficient, such as lead zirconate titanate (PZT), are rigid, fragile, and lack biocompatibility. These characteristics render their use in applications related to the human body challenging.

Piezoelectric polymers have been studied to develop stretchable sensors. Polyvinylidene fluoride (PVDF) is the most popular piezoelectric polymer material owing to its high piezoelectric performance, ductility, flexibility, and biocompatibility; however, it is still not stretchable. Therefore, structural design is often studied to attain stretchability¹⁵. Kirigami^{16–19}, honeycomb^{20–22}, and helical^{23–25} structures, as well as metamaterials²⁶ that enable stretching, have been studied. Kirigami structures, or paper cutting patterns, have more expansive design freedom than other approaches, making it easy to fabricate sensors with different performances. However, existing studies on kirigami structures employed old-fashioned fabrication methods, such as using a cutter knife^{10,27,28}, producing sensors with limited applications^{29–31}, low sensor performance^{29,32}, and low stretchability^{28,33}.

Here, a kirigami design was adopted to create a stretchable sensor using a rigid PVDF film. A stretchable strain sensor with tunable properties was fabricated using the kirigami design. The pattern was designed using finite element analysis (FEA) to achieve target performance. The FEA results also facilitate the understanding of sensor property with stress distribution. In addition, a measurement circuit was designed to measure the actual voltage generated by the sensor. The output voltage peak was maintained and can be used for strain sensing. The electromechanical properties of the sensor with different kirigami designs were analyzed. Sensor properties were evaluated and compared for every pattern. It was found that a kirigami piezoelectric strain sensor can achieve high levels of stretchability and sensitivity. Finally, the sensor was successfully applied to a

¹Department of Mechanical Engineering, Seoul National University, Gwanak-ro 1, Gwanak-gu, Seoul 08826, Republic of Korea. ²MX Division, Samsung Electronics, Samsungro 129, Suwon-si, Gyeonggi-do 16677, Republic of Korea. ³Department of Mechanical Engineering, Dankook University, Jukjeon-ro 152, Suji-gu, Yongin 16890, Republic of Korea. ⁴Institute of Advanced Machines and Design, Seoul National University, Gwanak-ro 1, Gwanak-gu, Seoul 08826, Republic of Korea. ⁵These authors contributed equally: Young-Gyun Kim, Ji-Hyeon Song. ✉email: ahnsh@snu.ac.kr

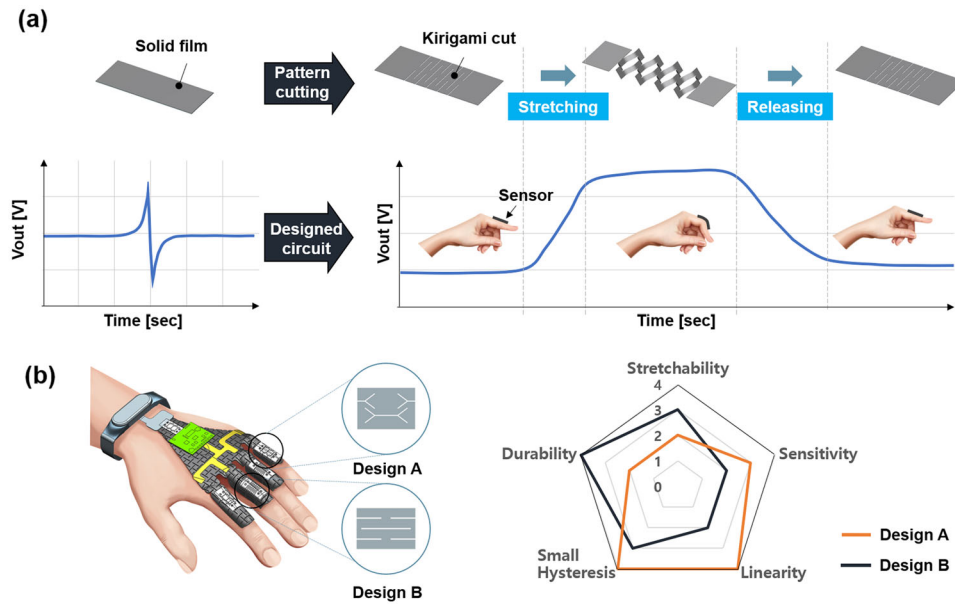


Fig. 1 Concept of the kirigami piezoelectric strain sensor. **a** Strain sensing mechanism. **b** Sensor property design with kirigami patterns.

wearable sensor by implementing a haptic glove, and playing the piano was demonstrated.

RESULTS

Strain sensor design and fabrication

Figure 1 shows the working mechanism of the kirigami piezoelectric strain sensor. The piezoelectric film was cut using a kirigami pattern, and the structural distortion of each cut segment resulted in stretchability. As the fabricated sensor uses a piezoelectric material, the generated output voltage can be measured to detect the strain. The voltage decreases to zero when the strain is removed. Typically, the voltage peak generated by the piezoelectric materials cannot be measured because it disappears within a short period of time. The output voltage can be measured accurately and maintained for a certain period using the designed circuit. This feature enables the usage of piezoelectric materials as strain sensors. Figure 1a depicts a wearable sensor attached to the fingers. The sensors stretch when the fingers are curled and return to their original shape when they unfold. Thus, motion can be detected by analyzing the output voltage. Figure 1b shows the advantages of the kirigami piezoelectric strain sensor. Sensors with different kirigami designs have different properties, including stretchability, sensitivity, linearity, hysteresis, and durability. The kirigami pattern can be designed to meet the requirements of the target properties for different applications, and different sensing properties can be achieved with different kirigami patterns to target different body parts.

Figure 2 shows the design and fabrication of a kirigami piezoelectric strain sensor. Figure 2a depicts the fabrication of the sensor and its layered structure. A nanosecond ultraviolet (UV) laser process was used to ablate the film. The laser scanner facilitates the ablation process for different designs, including a fine structure with a micrometer scale. The polarized PVDF film was coated with poly(3,4-ethylenedioxythiophene) (PEDOT), carbon nanotubes (CNTs), and Ag electrodes on both sides. Polyethylene terephthalate (PET) films increased the mechanical properties and durability of the fabricated sensor. The PET substrate was attached with an electrode coated PVDF film with an adhesive layer (thickness: 10 μm). The Young's modulus of the adhesive layer was 0.02 GPa, which is lower than that of PET (3 GPa) and PVDF film (0.8 GPa). Therefore, the friction or slip

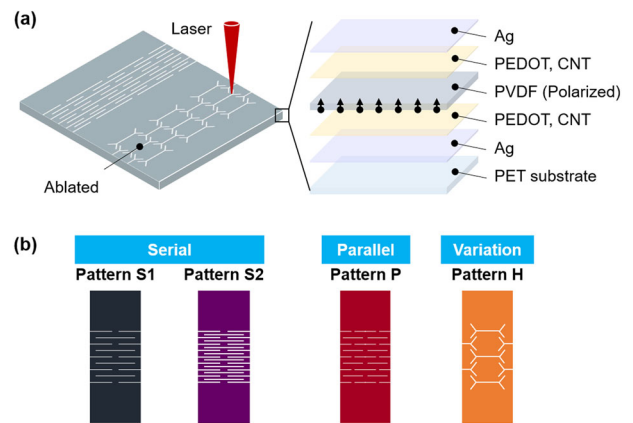


Fig. 2 Fabrication of kirigami patterns. **a** Laser cutting process and layer structure of the sensor. **b** Kirigami patterns.

occurring between the PVDF film and PET substrate was absorbed by the adhesive layer. The cyclic test was conducted with and without PET substrate to evaluate the zero-shifting phenomena. The results can be found in Supplementary Information. Zero shifting phenomena were observed in both cases, showing that the substrate is not related to the phenomena. This is because of the low-frequency noise induced by the heat from the surroundings³⁴.

Figure 2b shows the four kirigami patterns that were designed and tested. Kirigami cuttings of 2-1-2-1 and 3-2-3-2 were called serial and parallel patterns, respectively. Parallel patterns were designed to increase the stress applied to the film. Eight and sixteen segments (denoted as patterns S1 and S2, respectively) were cut for the serial pattern. The distance between the segments was 1.25 and 0.625 mm for S1 and S2, respectively. Eight segments were cut for the parallel pattern, which is denoted as pattern P. The size and distance between cuts were determined to meet the required size and stretchability based on the target applications. The kirigami design variations were also tested. The honeycomb structure was denoted as pattern H. Pattern H has the Y-shape cut at the edge of the cut in a serial pattern, distributing the stress concentration from point to line. Despite the different

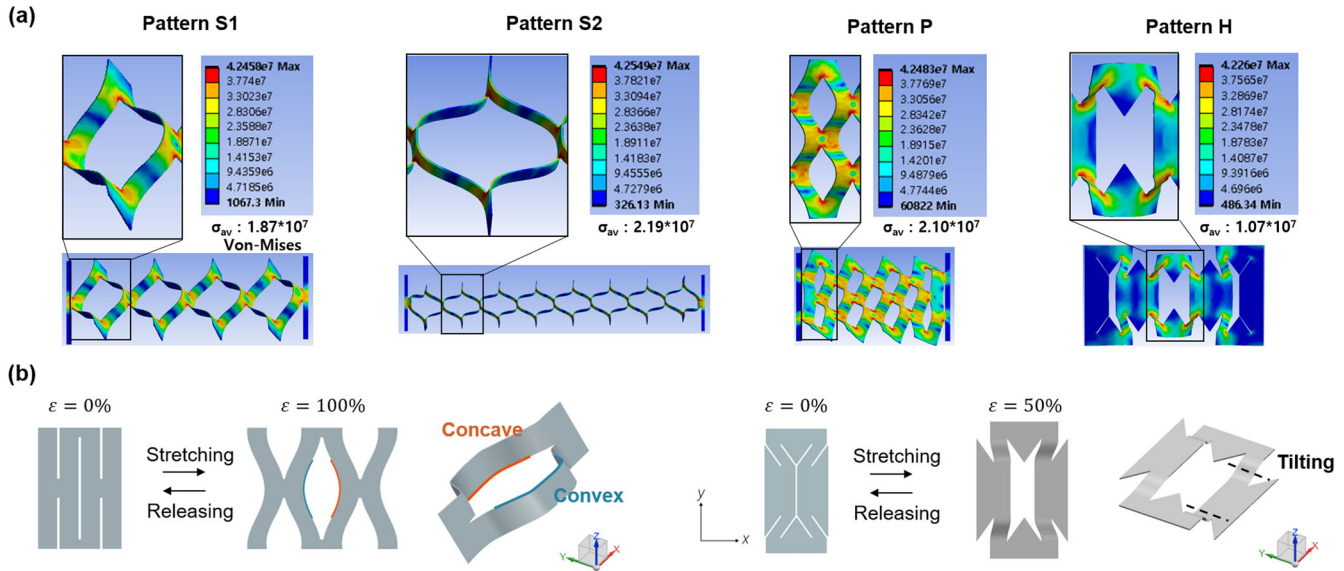


Fig. 3 Modeling of the kirigami patterns. **a** Finite element analysis of the kirigami pattern. **b** Structural distortion to attain stretchability of pattern S, P, and H.

patterns, the overall size of the kirigami sensor was the same, facilitating a fair comparison of the piezoelectric performance under the same conditions.

Pattern design using FEM analysis

FEA was conducted to analyze the stress distribution of the PVDF film under different strains. The results were used to correlate and design the sensor properties with the stress distribution. Figure 3a shows the FEA results of patterns S1, S2, P, and H obtained using Ansys software. It depicts the stretched state of the film as well as the stress value when stretched to the maximum strain depending on the pattern design. The maximum strain is determined considering the durability of the strain sensor and the limitation of the fabrication process. A longer cut can increase the maximum strain; however, the smaller margin results in low durability. The limitation of the fabrication process is detailed in the Discussion. The details of the simulation are described in the Methods section. The stretchability is attained by the structural distortion of the segments. The segment is bent in the convex and concave directions in patterns S and P, as shown in Fig. 3b. However, pattern H has a different distortion mechanism than patterns S and P. The segment is tilted by the line structure when pattern H is stretched. The tilting of the segment hinged along the dotted line in Fig. 3b for pattern H results in stretchability. When the segment is under a bending motion, stress is applied in the lateral direction. Therefore, the piezoelectric strain sensor is operated in the d_{31} mode.

Patterns S1, S2, and P have distributed stress, whereas pattern H has concentrated stress. The averaged stress applied on the structure by von Mises criteria is 2.19×10^7 , 2.10×10^7 , 1.87×10^7 , and 1.07×10^7 N/m² for patterns S2, P, S1, and H, respectively, when the maximum strain is applied. Pattern S2 has a higher stress because of its high stretchability. Pattern P has a higher stress than other patterns when the same strain is applied. Thus, pattern P has a higher sensitivity but lower durability than patterns S1, S2, and H.

The stress is not distributed over the segment surface in pattern H. Instead, it is concentrated on the line and edge of the cutting. Therefore, pattern H will have a low stretchability compared to patterns S1 and S2. However, even a small deformation triggers the tilting of the large segment parts, and the stress is focused on

a certain part of the pattern. This phenomenon can be compared to a lever, where a small force can induce a large deformation. Therefore, pattern H is expected to have a high sensitivity. In addition, the sensor performance is highly linear because the tilting motion is linear. We can easily predict and design the electromechanical properties of the piezoelectric sensors with different structures using FEA.

Electromechanical properties of the strain sensor

Figure 4 depicts the mechanical and electromechanical properties of the fabricated strain sensor. Figure 4a shows the stress–strain curve measured using a universal testing system to analyze the mechanical properties of strain sensors with different patterns. Three samples were tested, and the average values of the measurements were plotted. The sample was tested until the film was torn. However, only the data prior to the plastic deformation were obtained and plotted because the sensor could not be used after plastic deformation. The maximum stretchability and Young's modulus vary with the different pattern designs. Pattern S2 exhibited the highest stretchability (320.8%), whereas pattern P exhibited the lowest. However, pattern P showed a larger Young's modulus than the other patterns. Figure 4b presents the output voltage as a function of strain. For each pattern, three samples were tested for five repeated stretching and releasing cycles, and the measured data were averaged. Pattern P had the highest output voltage (2.23 V) when 0.25 strain was applied. Patterns S1 and P had higher output voltages than patterns S2 and H. The output voltage is related to the applied stress when stretched. The experimental results match with FEM analysis; pattern S1 and P have high averaged stress; therefore, they have high output voltage. Pattern H has the lowest average stress; therefore, it has the lowest output voltage. Pattern S2, however, has the highest stress but lower output voltage compared to patterns S1 and P. This is because the output voltage is calculated as

$$\sigma_1 d_{31} + \sigma_2 d_{32} + \sigma_3 d_{33} \quad (1)$$

where, σ_1 , σ_2 , and σ_3 are the stress applied on x, y, and z-axis d_{31} , d_{32} , and d_{33} are the piezoelectric coefficient in x, y, and z-axis when the materials are polarized in z-axis direction. d_{31} , d_{32} , and d_{33} values are 22, 2, and 35 pC/N for PVDF film. Von-Mises criteria

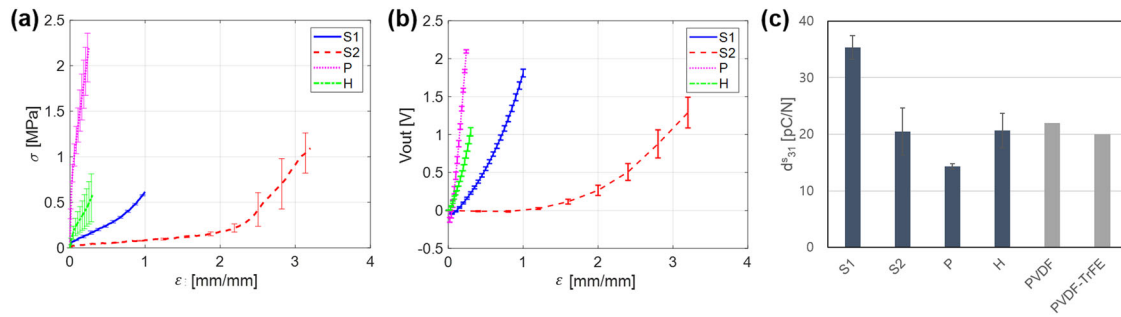


Fig. 4 Mechanical and electromechanical properties of the fabricated strain sensor. a Stress–strain curve. **b** Output voltage with strain. **c** Calculated d_{31}^s value compared with the original solid film. The error bars represent the standard deviation of the data.

σ_{VM} calculates as

$$\sigma_{VM} = \sqrt{\frac{1}{2} \left[(\sigma_2 - \sigma_3)^2 + (\sigma_3 - \sigma_1)^2 + (\sigma_1 - \sigma_2)^2 \right]}. \quad (2)$$

Therefore, averaged stress analyzed with FEM results cannot exactly predict the experimental values because different piezoelectric coefficients along different axes are not considered. The measured data were used to calculate the sensitivity of the strain sensor, as discussed in the following section. Figure 4c shows the d_{31}^s values of the strain sensor for different kirigami patterns. d_{31}^s is defined as

$$d_{31}^s = dQ/dF * A_1/A_3 = \frac{dQ}{d\epsilon} \frac{d\epsilon}{dF} \frac{A_1}{A_3}, \quad (3)$$

where Q is the electric charge and F is the stress³⁵. A_1 and A_3 are the cross-sectional areas in the x - and z -directions, respectively, and ϵ is the applied strain. $dQ/d\epsilon$ can be obtained from the strain-output voltage curve, as shown in Fig. 4b. $d\epsilon/dF$ can be obtained from the stress–strain curve, as depicted in Fig. 4a. Therefore, dQ/dF can be calculated based on the mechanical and electromechanical properties of the sensor. The calculated data of different patterns and the PVDF film in the bulk state were compared. The comparison results showed that the piezoelectric coefficient could be tailored using different kirigami pattern designs. Pattern S1 had the highest d_{31}^s value (35.34), whereas pattern P had the lowest (14.32). The pattern S1 had a higher d_{31}^s value than the original PVDF film. The patterns S2 and H had similar d_{31}^s values compared to the bulk poly(vinylidene fluoride-co-trifluoroethylene) (PVDF-TrFE)³⁶.

Circuit design

Figure 5 depicts the designed circuit for the piezoelectric strain sensor. Typically, the data acquisition apparatus is directly attached to the piezoelectric sensor, as shown in Fig. 5a. However, when the sensor is stretched and released, the signal is not large and clear because of the noise. The maximum output voltage was approximately 0.02 V. An op-amp with a voltage follower was included to measure the sensor output accurately. It prevented voltage loss due to the internal resistance of the measurement circuit. Therefore, the output signal from the sensor could be accurately measured. The signal was amplified and could be differentiated from the noise. Usually, a parallel resistor in the circuit drains the remaining voltage from the circuit. This resulted in the dissipation of the voltage in a short time period, displayed as the sharp peak in Fig. 5b. If the output signal is highly transient, it is difficult to measure the sensor output. Therefore, the parallel resistor is excluded from the circuit shown in Fig. 5c. The maximum output voltage was measured as 1.73 V using this circuit and remained stable for a certain period of time. If the strain is maintained, the voltage is maintained for a certain period of time. The slow voltage drop is due to charge loss caused by the internal

resistance. The relaxation rate was 7.76×10^{-4} V/sec. The dynamic response of the sensor can be found in Supplementary Information. Therefore, the improved circuit design enabled accurate and consistent measurement of the output voltage from the piezoelectric materials for strain sensor applications with a two-order higher magnitude than the regular circuits. A detailed mathematical analysis of the circuit showing the different graphs for different circuit designs is in Supplementary Information.

Sensing properties of the strain sensor

The fabricated kirigami piezoelectric strain sensors were characterized to evaluate their properties. The maximum stretchability, sensitivity, linearity, hysteresis, and durability were measured and compared. The maximum stretchability was measured immediately before the film began to tear. The sensitivity was defined as $dV/d\epsilon$. The sensor sensitivity was normalized to the sample area for comparison to other studies. Figure 6a shows a comparison of the stretchability and sensitivity of the kirigami piezoelectric strain sensors with different patterns^{10,11,28,29,32,33}. There exists a trade-off relationship between stretchability and sensitivity. The sensitivities of patterns P and H were 9.14 and 3.48 V/cm², respectively. The highest stretchability (320.8%) was observed for S2. Structural depolarization was conducted for pattern P to improve the sensitivity further, as shown in Fig. 6b. Pattern P attains stretchability using the concave and convex bending of each segment, as discussed above. Different segment parts are under tension and compression, as marked by red and blue, respectively, in Fig. 6b. The output currents generated from different segments have different directions, resulting in a lower total output voltage. Therefore, thermal depolarization was conducted for the segments with compression to remove the piezoelectric performance. The thermal depolarization was conducted by a laser process. The laser was not strong enough to cut the film but raised the surface temperature to the Curie temperature, removing the piezoelectric characteristics. This process is described in detail in Methods. Pattern P shows increased sensitivity of 9.86 V/cm² with structural depolarization.

The results were also compared to those of other studies in which kirigami patterns were used in piezoelectric strain sensors. The highest sensitivity of 6.57 V/cm² was obtained in the work of Sun et al.¹¹, whereas Zhou et al.³² reported the highest stretchability of 300%. This research successfully produced kirigami piezoelectric sensors with a higher stretchability and higher sensitivity than previously reported.

The linearity was calculated from the data in Fig. 4b. The output voltage is proportional to the strain. The linearity value is defined as the R-squared value obtained from the plot of the initial voltage to the peak voltage versus strain. Figure 6c shows the linearity of the sensors. The sensors showed high linearity for values ranging from 0.9683 to 0.9824, with the exception of pattern S2. Pattern S2 had the lowest linearity of 0.7914. Pattern H had the highest linearity among the samples, as expected from the FEM results. In

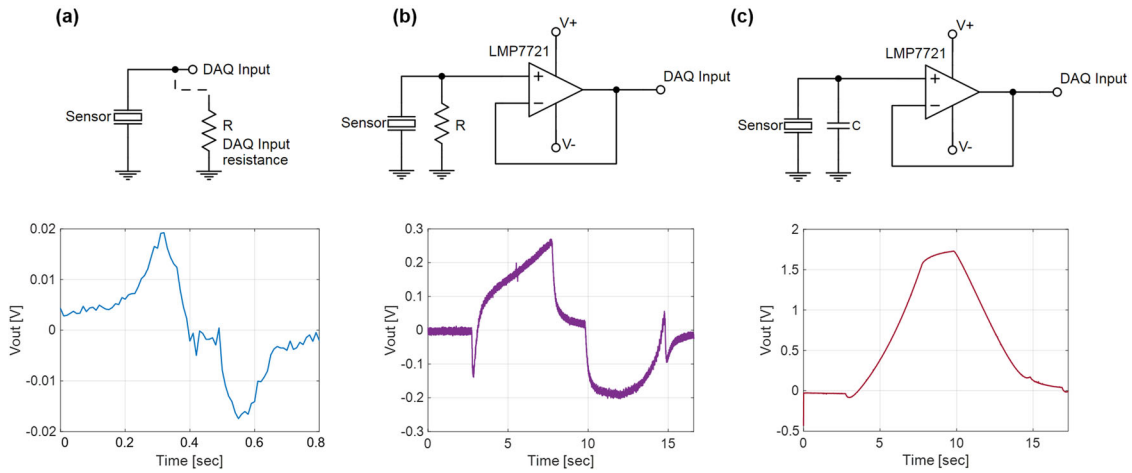


Fig. 5 **Circuit design.** **a** Original data acquisition circuit and its output signal. **b** Circuit with op-amp and voltage follower and its output signal. **c** Circuit with op-amp and voltage follower and without parallel resistance and its output signal.

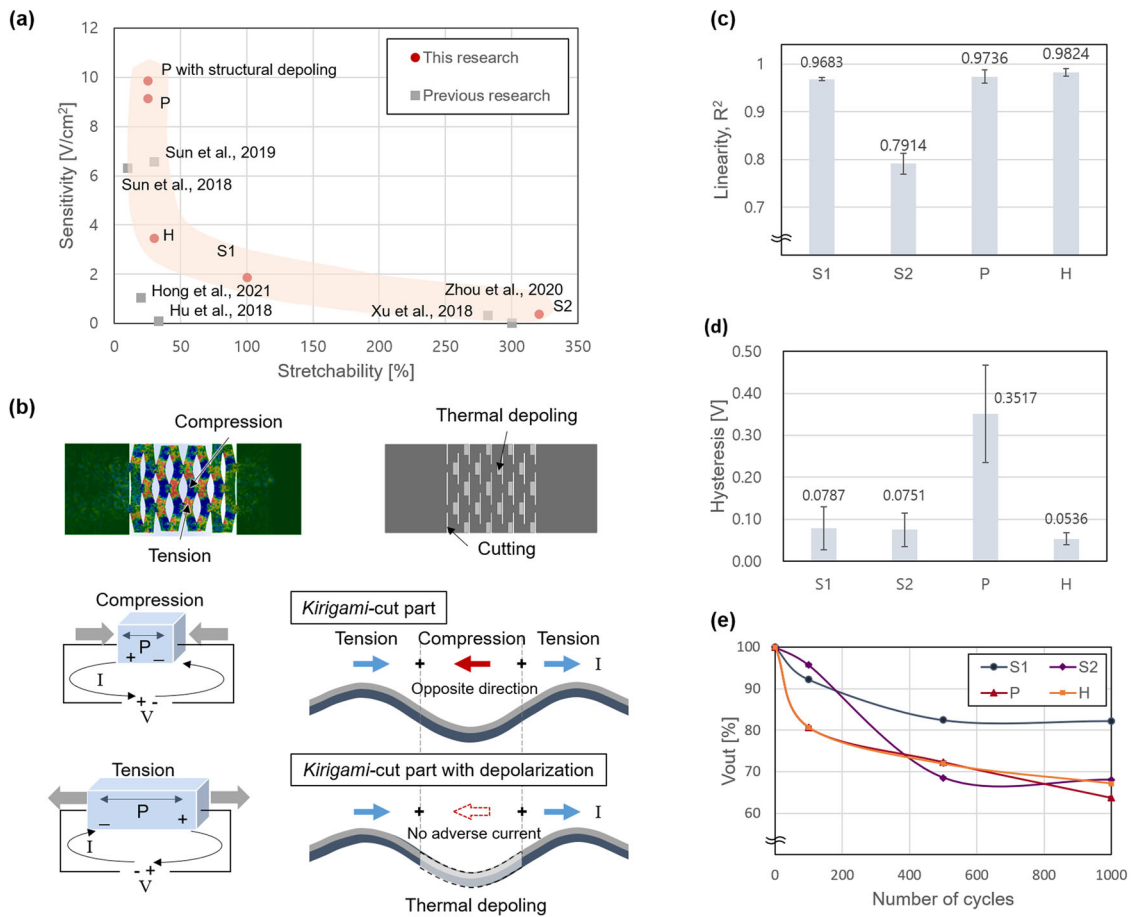


Fig. 6 **Comparison of the strain sensor properties.** **a** Stretchability and sensitivity. **b** Improving sensitivity using structural depolarization. **c** Linearity. **d** Hysteresis. **e** Durability. The error bars represent the standard deviation of the data.

addition, the hysteresis was calculated as the difference between the initial and released voltages. The hysteresis can be analyzed using the graph of output voltage vs. time. The data can be found in the Supplementary Information. The output voltage increases as the sensor is stretched but does not directly drop to the initial voltage value when it is released, as shown in Fig. 1a. The output voltage initially decreases linearly (known as the releasing region)

to a certain voltage (known as the released voltage) and then slowly decreases to the initial voltage. Therefore, the hysteresis was evaluated from the difference between the initial and released voltages. The releasing region was determined as the time period when the voltage value is linearly related to the peak voltage. The linear region was determined with an R-squared value of 98%. Figure 6d shows the hysteresis of the sensors. Lower

hysteresis values are desirable for strain sensor applications. Pattern H has lower hysteresis compared to other patterns, whereas pattern P has higher hysteresis. The hysteresis is affected by the elastic–plastic region of the sample. If the stress is not removed instantly, the voltage value exists until the stress is slowly removed and the sample returns to its original shape. The yield strength of a PVDF film is 50 MPa³⁷. As the material of pattern P is subjected to a relatively higher stress, as shown in the FEM results in Fig. 3, it is more likely to go through the elastic–plastic region, explaining the high hysteresis.

The durability of the sensor was evaluated using a cyclic test. The stretching and releasing motions were repeated for 1000 cycles for each pattern. The stretching motion (up to 50% of the maximum stretchability) was performed for each pattern during the cyclic test, and the results are shown in Fig. 6e. The output voltage was measured when the sample was stretched with repeated stretching and releasing motions. This was compared with that of the initial cycle. Three samples were tested, and an average value was plotted. Most of the designed sensors exhibited a stable performance even after 1000 repeated stretching tests, showing a decrease in performance ranging from 63.74 to 82.23%. In addition to the output voltage value, saturation is an important factor for sensor applications. If the graph tends to saturate, the sensor exhibits reliable performance even after an additional stretching test. The decreasing region can be regarded as the sensor-aging region. The pattern S1 has saturated trends with a voltage of 82.43 and 82.23% of the initial value after 500 and 1000 cycles, respectively, corresponding to a change of 0.20%. Pattern S2 also shows reliable performance. However, pattern P exhibits a non-uniform trend, showing a decrease of 8.63% from 500 to 1000 cycles.

Application to a VR haptic glove

Finally, the fabricated sensor was applied to a wireless haptic glove for playing musical instruments using VR applications. The advantage of the developed sensor is in its tunability and its simple fabrication process. The ring and pinky fingers have a lower strain compared to the index and middle fingers based on physiology. In addition, the pinky finger tends to bend along with the ring finger when it is completely bent. Therefore, a small

movement of the pinky finger should be recognized to separate the signal. If the movement characteristics of each body part were ignored and the same sensor was applied, the stretchability and sensitivity will not be appropriate for each body part, leading to sensing errors. Therefore, the movement behavior, including the range and force, was considered by selecting the appropriate sensor performance, as shown in Fig. 7a. Pattern S1, which has a high stretchability and reasonable sensitivity, was selected for the index and middle fingers. A sensor with high sensitivity and linearity is required to detect small movements of the finger for the ring and pinky fingers. Durability is also required for stable performance in real-world applications for an extended time. Therefore, pattern H was chosen for the ring and pinky fingers. The sensor was attached to the finger and connected to a printed circuit board, as shown in Fig. 7b. The microprocessor, relay, and Bluetooth module were connected, and the piano was successfully played using these two sensor types. Figure 7c shows the output voltage signal of the glove received by a PC via Bluetooth communication with the movement of each finger while playing music. Each finger movement was detected successfully, and a musical note was played accordingly. The duration of the bent state controlled the duration of the sound, and the speed of finger movement controlled the volume. “Arirang” and “Amazing Grace” musical notes were played successfully. A link to the video can be found in the Supplementary Information. This approach can be applied to other VR applications, such as drone controllers and VR keyboards. It can also be extended to other body parts, such as the neck and knee, using an appropriately designed sensor.

DISCUSSION

Different kirigami patterns show different sensing performances, and the overall sensor properties were compared. Pattern S1 showed good performance for most properties, particularly for durability. However, it exhibited a low sensitivity. Pattern S2 demonstrated excellent stretchability and good durability, whereas it had low sensitivity and linearity. Pattern P showed good sensitivity and linearity. However, it lacked durability, hysteresis, and stretchability. Pattern H exhibited high linearity and sensitivity with good hysteresis and durability but lacked stretchability.

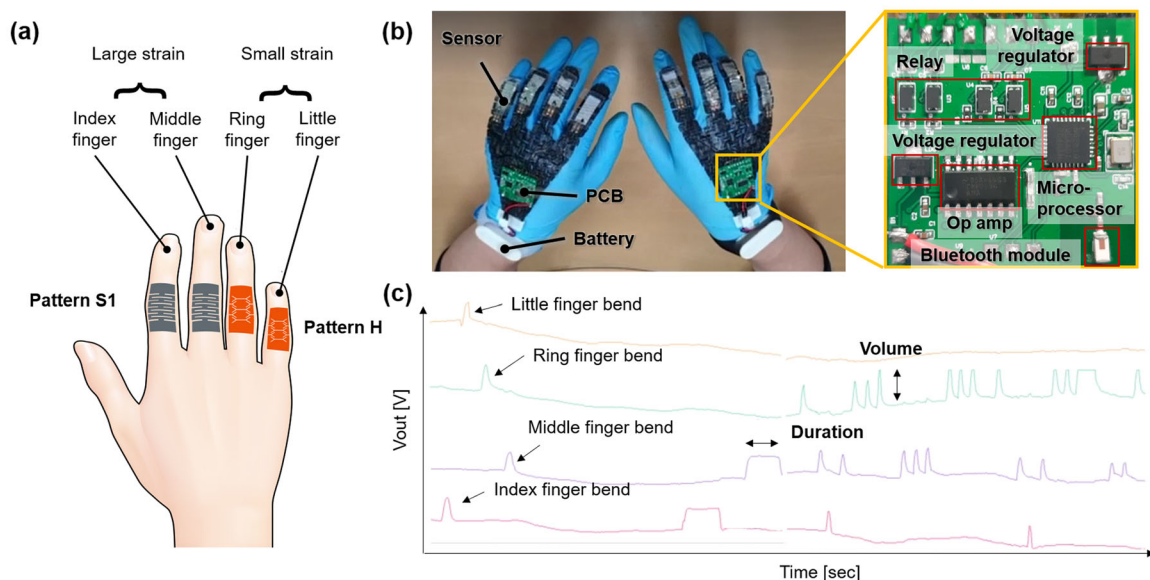


Fig. 7 Application to a VR haptic glove. **a** Sensor selection considering movement behavior of body and sensor performance. **b** Fabricated haptic glove and description of the printed circuit board. **c** Output voltage signal with the movement of each finger while playing a musical instrument.

Likewise, different kirigami patterns have different sensor properties. The structural design determines the stress distribution under the application of strain. The maximum output voltage and the shape of the graph vary depending on the stress distribution—higher stress results in a higher sensitivity. However, if the maximum stress reaches the yield strength of the material, the sensor exhibits a high hysteresis; moreover, the durability decreases. Linearity is related to the type of structural deformation. If the deformation is linear with no curve structure deformation, the linearity of the sensor increases.

The mechanical and electromechanical properties were analyzed for different kirigami patterns. Based on our analysis, a pattern with fewer or shorter length cuts has higher Young's modulus and lower stretchability. For example, pattern S1 has a lower stretchability than pattern S2 because it has fewer cuts. In addition, pattern P has a lower stretchability than pattern S1 because its cuts are shorter. Electromechanical properties can also be designed. Using FEA, it is easy to design and understand the electromechanical properties of piezoelectric sensors with different structures by analyzing the stress distribution. The maximum strain, as well as the sensitivity, can be tuned by changing the kirigami design.

To fabricate the sensor kirigami patterns, a laser process with a laser beam diameter of 50 μm was used. The laser process has many advantages, such as precise cutting, curved cutting, design flexibility, and fast fabrication. The cutting mechanism of the nanosecond laser is based on heat damage. Therefore, heat inevitably affects the periphery of the laser beam spot. If there were too many cuts, the distance between the cuts is decreased, and the ratio of the heat-affected zone occupying the whole structure is increased. The Curie temperature of the PVDF film was 120 $^{\circ}\text{C}$, which is not high. The process temperature could reach up to 120 $^{\circ}\text{C}$ during the cutting process, and the piezoelectric performance of the materials could be lost, resulting in low sensing performance. In addition, if the fraction of the cutting area is increased, the mechanical properties of the film are degraded, leading to low durability. This behavior explains why the number of cuts in the single pattern was tested until 16, whereas a higher number of cuts could further increase the stretchability.

In summary, a stretchable piezoelectric strain sensor was developed by introducing a kirigami pattern to achieve stretchability in a rigid PVDF film. In addition, a circuit was designed to measure the output voltage of the piezoelectric strain sensor accurately and consistently. The sensing performance was tailored using the kirigami pattern design with the help of finite element analyses. The electromechanical properties of the sensors were analyzed, revealing that different kirigami patterns produce different sensing performances, such as maximum strain and sensitivity. Based on these analyses, it was concluded that a kirigami pattern with fewer or shorter length cuts has a lower stretchability and a higher stress concentration, resulting in enhanced sensitivity. Pattern H showed different distortion mechanisms and provided the highest linearity compared to patterns S1, S2, and P. An optimized sensor output circuit was designed and enabled an accurate output voltage measurement by amplifying the output 86.5 times higher than that of the original circuit. Therefore, a kirigami piezoelectric sensor was fabricated with a sensitivity of 9.86 V/cm^2 and stretchability of 320.8%, the highest values reported to data for kirigami piezoelectric strain sensors. The error included in the results was induced by deviations in the dimensions of the samples, which in turn were caused by the fabrication process. A laser process with higher resolution and more stable output energy could improve the quality of the cutting, thus minimizing such error. Finally, the fabricated sensor was successfully implemented in a haptic glove for playing musical instruments. The piezoelectric sensor discussed in this research can be further developed by adopting

more complicated kirigami patterns and aiming for miniaturization and transparency.

METHODS

Fabrication of a piezoelectric kirigami sensor

A PVDF film with a PEDOT + CNT electrode coating on both sides was purchased from Fils, Korea. The thickness of the film was 80 μm . An additional electrode was coated with Ag to ensure conductivity after stretching. The electrode was coated with Ag by E-beam evaporation at 2.0 A/s for 1000 seconds under a 3.0×10^{-7} MPa vacuum state. The thickness of the coated Ag electrode was 200 nm. A PET film was attached to increase the durability of the film. An ultraviolet nanosecond laser was used to cut the film according to the designed pattern. The pulse width and frequency of the laser system were 15 ns and 30 kHz, respectively. The laser power was 400 mW. The scan speed and number of scans were 40 mm/s and 20, respectively. For structural depolarization, 300 mW was used with 160 mm/s scan speed twice. An anisotropic conductive film was bonded to measure the electrical output of the system.

Measurement of the piezoelectric property

The electric properties were measured while a strain was applied to the film. The linear stage (Sigma-Koki, OSMS26-100) and stage controller (Sigma-Koki, GSC-01) were controlled by LABVIEW to apply strain to the film. The fabricated strain sensor was stretched at a speed of 2.5 mm/s. The sample was stretched to its maximum value. Before breakage, the maximum deformations were 100.10, 320.80, 25.04, and 30.04% for patterns S1, S2, P, and H, respectively. A data acquisition system (DAQ, National Instruments, NI-6009) and a voltage follower circuit composed of operational amplifiers (OP-amp, Texas Instruments, LMP7721) were used to measure the voltage output. The measurement system was programmed to collect data at a sampling rate of 100 Hz. Each design was tested on three samples with five tests for each sample. The average output voltage and its standard deviation were plotted.

Mechanical property measurements

The mechanical properties of the sensor were measured using a universal testing machine (Instron 5948 Microtester). The kirigami cut PVDF film was stretched at 0.15 mm/s until fracture. Three samples were tested for each kirigami design, and the stress–strain curve was plotted. The value of $dF/d\epsilon$ was calculated.

Finite element analysis

The FEA simulations were performed using commercial simulation software (Ansys) to analyze the stress distribution of different kirigami patterns. The kirigami piezoelectric strain sensor composed of a PVDF film (Young's modulus (E) = 0.62 GPa, Poisson's ratio (ν) = 0.35) and PET film (E = 2.5 GPa, ν = 0.37) were modeled. The force was applied until the deformation of the pattern reached the maximum value. The mesh size was scaled per part, and the minimum characteristic length of the mesh elements was 4.26, 3.54, 1.82, and 1.99 μm for patterns S1, S2, P, and H, respectively.

DATA AVAILABILITY

Data is available on request from the authors.

Received: 15 March 2022; Accepted: 27 May 2022;

Published online: 23 June 2022

REFERENCES

1. Yao, S. et al. Nanomaterial-enabled flexible and stretchable sensing systems: processing, integration, and applications. *Adv. Mater.* **32**, 1902343 (2020).
2. Wu, Y. et al. Piezoresistive stretchable strain sensors with human machine interface demonstrations. *Sens. Actuators A Phys.* **279**, 46–52 (2018).
3. Wang, X. et al. Highly sensitive and stretchable piezoresistive strain sensor based on conductive poly(styrene-butadiene-styrene)/few layer graphene composite fiber. *Compos. Part A Appl. Sci. Manuf.* **105**, 291–299 (2018).
4. Zhang, Q. et al. Highly sensitive and stretchable strain sensor based on Ag@CNTs. *Nanomaterials* **7**, 424 (2017).

5. Yan, W. et al. Giant gauge factor of Van der Waals material based strain sensors. *Nat. Commun.* **12**, 1–9 (2021).
6. Tan, C. et al. A high performance wearable strain sensor with advanced thermal management for motion monitoring. *Nat. Commun.* **11**, 1–10 (2020).
7. Xu, H. et al. An ultra-stretchable, highly sensitive and biocompatible capacitive strain sensor from an ionic nanocomposite for on-skin monitoring. *Nanoscale* **11**, 1570–1578 (2019).
8. Kim, S.-R., Kim, J.-H. & Park, J.-W. Wearable and transparent capacitive strain sensor with high sensitivity based on patterned Ag nanowire networks. *ACS Appl. Mater. Interfaces* **9**, 26407–26416 (2017).
9. Atalay, O. et al. A Highly Stretchable Capacitive-Based Strain Sensor Based on Metal Deposition and Laser Rastering. *Adv. Mater. Technol.* **2**, 1700081 (2017).
10. Sun, R. et al. Kirigami stretchable strain sensors with enhanced piezoelectricity induced by topological electrodes. *Appl. Phys. Lett.* **112**, 251904 (2018).
11. Sun, R. et al. Stretchable piezoelectric sensing systems for self-powered and wireless health monitoring. *Adv. Mater. Technol.* **4**, 1900100 (2019).
12. Khan, H., Razmjou, A., Ebrahimi Warkiani, M., Kottapalli, A. & Asadnia, M. Sensitive and flexible polymeric strain sensor for accurate human motion monitoring. *Sensors* **18**, 418 (2018).
13. Soury, H. et al. Wearable and stretchable strain sensors: materials, sensing mechanisms, and applications. *Adv. Intell. Syst.* **2**, 2000039 (2020).
14. Yin, B., Liu, X., Gao, H., Fu, T. & Yao, J. Bioinspired and bristled microparticles for ultrasensitive pressure and strain sensors. *Nat. Commun.* **9**, 1–8 (2018).
15. Vallem, V., Sargolzaeiavai, Y., Ozturk, M., Lai, Y.-C. & Dickey, M. D. Energy harvesting and storage with soft and stretchable materials. *Adv. Mater.* **33**, 2004832 (2021).
16. Song, Z. et al. Kirigami-based stretchable lithium-ion batteries. *Sci. Rep.* **5**, 1–9 (2015).
17. Isobe, M. & Okumura, K. Initial rigid response and softening transition of highly stretchable kirigami sheet materials. *Sci. Rep.* **6**, 1–6 (2016).
18. Xu, K. et al. Highly stable kirigami-structured stretchable strain sensors for per-durable wearable electronics. *J. Mater. Chem. C* **7**, 9609–9617 (2019).
19. Won, P. et al. Stretchable and transparent kirigami conductor of nanowire percolation network for electronic skin applications. *Nano Lett.* **19**, 6087–6096 (2019).
20. Lv, Z. et al. Honeycomb-Lantern-Inspired 3D Stretchable Supercapacitors with Enhanced Specific Areal Capacitance. *Adv. Mater.* **30**, 1805468 (2018).
21. Pu, J., Wang, X., Xu, R. & Komvopoulos, K. Highly stretchable microsupercapacitor arrays with honeycomb structures for integrated wearable electronic systems. *ACS Nano* **10**, 9306–9315 (2016).
22. Kang, S. et al. Stretchable lithium-ion battery based on re-entrant micro-honeycomb electrodes and cross-linked gel electrolyte. *ACS Nano* **14**, 3660–3668 (2020).
23. Won, Y., Kim, A., Yang, W., Jeong, S. & Moon, J. A highly stretchable, helical copper nanowire conductor exhibiting a stretchability of 700%. *NPG Asia Mater.* **6**, e132–e132 (2014).
24. Cheng, M.-Y., Tsao, C.-M., Lai, Y.-Z. & Yang, Y.-J. The development of a highly twistable tactile sensing array with stretchable helical electrodes. *Sens. Actuators A Phys.* **166**, 226–233 (2011).
25. Shang, Y. et al. Self-stretchable, helical carbon nanotube yarn supercapacitors with stable performance under extreme deformation conditions. *Nano Energy* **12**, 401–409 (2015).
26. Dorsey, K. J. et al. Atomic layer deposition for membranes, metamaterials, and mechanisms. *Adv. Mater.* **31**, 1901944 (2019).
27. Fang, L., Li, J., Zhu, Z., Orrego, S. & Kang, S. H. Piezoelectric polymer thin films with architected cuts. *J. Mater. Res.* **33**, 330–342 (2018).
28. Hu, N. et al. Stretchable kirigami polyvinylidene difluoride thin films for energy harvesting: design, analysis, and performance. *Phys. Rev. Appl.* **9**, 21002 (2018).
29. Xu, R. et al. Kirigami-inspired, highly stretchable micro-supercapacitor patches fabricated by laser conversion and cutting. *Microsyst. Nanoeng.* **4**, 1–10 (2018).
30. Morikawa, Y. et al. Ultrastretchable kirigami bioprobes. *Adv. Healthc. Mater.* **7**, 1701100 (2018).
31. Yong, K. et al. Kirigami-inspired strain-insensitive sensors based on atomically-thin materials. *Mater. Today* **34**, 58–65 (2020).
32. Zhou, X. et al. All 3D-printed stretchable piezoelectric nanogenerator with non-protruding kirigami structure. *Nano Energy* **72**, 104676 (2020).
33. Hong, Y. et al. Highly anisotropic and flexible piezoceramic kirigami for preventing joint disorders. *Sci. Adv.* **7**, eabf0795 (2021).
34. Li, J. W. et al. Thermal effect on piezoelectric stick-slip actuator systems. *Rev. Sci. Instrum.* **79**, 046108 (2008).
35. Senturia, S. D. *Microsystem design*. (Springer Science & Business Media, 2007).
36. Cao, X. et al. Piezoelectric Nanogenerators Derived Self-Powered Sensors for Multifunctional Applications and Artificial Intelligence. *Adv. Funct. Mater.* **2021**, 2102983 (2021).
37. Srivastava, A., Jana, K. K., Maiti, P., Kumar, D. & Parkash, O. Poly (vinylidene fluoride)/CaCu₃Ti₄O₁₂ and La doped CaCu₃Ti₄O₁₂ composites with improved dielectric and mechanical properties. *Mater. Res. Bull.* **70**, 735–742 (2015).

ACKNOWLEDGEMENTS

This work was supported by the National Research Foundation of Korea (NRF) grant funded by the Korea Government (MSIT) (NRF-2021R1A2B5B03087094, NRF-2021R1G1A1093618, NRF-2021R1A4A2001824)

AUTHOR CONTRIBUTIONS

Y.G.K. and J.H.S. contributed to the research equally. Y.G.K. conceived and designed the analysis, contributed data and analysis tool and collected the data. J.H.S. conceived and designed the analysis, performed the analysis and wrote the paper. S.H. collected the data, contributed data and analysis tools, and performed the analysis. S.H.A. supervised the overall research process.

COMPETING INTERESTS

The authors declare no competing interests.

ADDITIONAL INFORMATION

Supplementary information The online version contains supplementary material available at <https://doi.org/10.1038/s41528-022-00186-4>.

Correspondence and requests for materials should be addressed to Sung-Hoon Ahn.

Reprints and permission information is available at <http://www.nature.com/reprints>

Publisher's note Springer Nature remains neutral with regard to jurisdictional claims in published maps and institutional affiliations.



Open Access This article is licensed under a Creative Commons Attribution 4.0 International License, which permits use, sharing, adaptation, distribution and reproduction in any medium or format, as long as you give appropriate credit to the original author(s) and the source, provide a link to the Creative Commons license, and indicate if changes were made. The images or other third party material in this article are included in the article's Creative Commons license, unless indicated otherwise in a credit line to the material. If material is not included in the article's Creative Commons license and your intended use is not permitted by statutory regulation or exceeds the permitted use, you will need to obtain permission directly from the copyright holder. To view a copy of this license, visit <http://creativecommons.org/licenses/by/4.0/>.

© The Author(s) 2022